

# Out of Equilibrium behaviour in topologically ordered systems on a lattice: fractionalised excitations and kinematic constraints

Claudio Castelnovo  
TCM group  
Cavendish Laboratory, University of Cambridge  
Cambridge, CB3 0HE, United Kingdom

December 27, 2014

These lecture notes touch upon aspects of out of equilibrium behaviour in topologically ordered systems, broadly interpreted. It should be noted that the selection of topics reflects a personal choice and it is not intended as a systematic review. Hopefully, these notes will stimulate the appetite of the interested reader to pursue further study in this area of research.

## 1 Topological order, broadly interpreted

Firstly, one should point out that these lectures do not aim to introduce nor adhere to a specific and accurate definition of *topological order*. Other lectures in this school may serve the purpose. Here, “topologically ordered systems” refer very loosely to systems that do not develop a local order parameter at low temperature (e.g., symmetry breaking) and yet exhibit non-trivial global properties.

Within this broad definition, which encompasses classical statistical mechanical systems as well as quantum mechanical systems, we shall take topologically ordered systems to be characterised by the following properties:

1. the lack of a local order parameter characterising the low temperature phase; rather, these system remain in a disordered ‘liquid’ state with non-trivial non-local correlations;
2. the collective excitations of the low temperature phase take the form of point-like quasiparticles that carry a fraction of the microscopic degrees of freedom in the system.

It is often the case that the low temperature phase can be effectively interpreted as a special *vacuum*, capable of hosting the emergent collective excitations as it *elementary particles*.

The properties of the emergent excitations and those of the vacuum are closely related. From a dynamical perspective, the vacuum determines both at the local as well as global (topological) level the rules of motion of the excitations. Vice versa, as the quasiparticles move across the system, they change it. The excitations act indeed as dynamical facilitators, as it is through their motion that the system can respond to external perturbations and/or relax to equilibrium.

The close interplay between excitations and their vacuum is often responsible for non-trivial and interesting dynamical properties, in particular when the system is driven out of equilibrium. This is a rich and interesting regime, controlled by the interplay of many (often independently tuneable) factors, such as the interactions between the emergent quasiparticles; the local and global kinematic constraints imposed by the vacuum; as well as, in quantum mechanical systems, the mutual statistics of the excitations.

For the reader who may be familiar with these models, examples include: lattice dimer models; vertex models (e.g., the six and eight vertex models in 2D, and spin ice in 3D); and the toric code model and Kitaev's model.

In these lectures, we will discuss specifically the case of classical spin ice (Sec. 2) and the quantum toric code (Sec. 3). The combination of strongly correlated physics, topological order, and far from equilibrium behaviour is generally a tall order. Within classical system, we will see that one can make substantial progress in understanding the dynamics, in particular following thermal and field quenches, thanks to an effective modelling of the vacuum and its emergent excitations. At the quantum mechanical level, a similar modelling is not readily available and the depth of our present understanding is limited to the modelling of leading energy barriers and asymptotic behaviour. We close with the discussion of an intriguing parallel that can be drawn between the toric code Hamiltonian and a class of lattice systems known as Kinetically Constrained Models, which were designed to achieve trivially disordered low temperature phases with emergent *long relaxation time scales* (Sec. 3.4).

## 2 Example 1: (classical) spin ice

In Sec. [\[Chalker lectures\]](#) you have seen how the behaviour of spin ice models and materials at low temperature can be understood as a spin liquid “vacuum” with an emergent gauge symmetry (inherited from the 2in-2out local constraint that minimises the energy). This vacuum hosts classical fractionalised excitations that take the form of free magnetic charges in three dimensions, or emergent magnetic monopoles. (For a review, see for instance Refs. [21, 20].)

As a first approximation, the collective behaviour of these systems at low temperature (Fig. 1) resembles that of a Coulomb liquid or pair plasma (i.e., a gas of positive and negative Coulomb-interacting point charges, which is overall neutral) [18]. Such effective description goes indeed a long way to capture the low-temperature behaviour of spin ice, with far less effort than would otherwise be required by conventional theoretical approaches for strongly correlated magnetic systems on a 3D lattice.

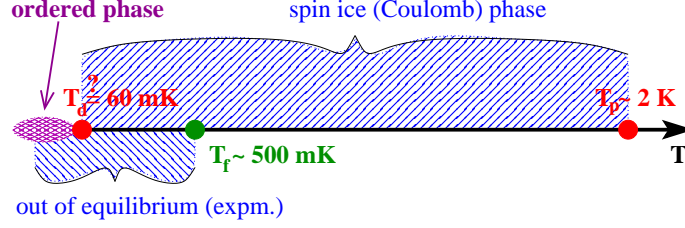


Figure 1: Schematic illustration of the different temperature regimes in spin ice. The theoretically predicted ordering transition at  $T_d$  appears to be prevented in experiments by freezing of the magnetic degrees of freedom below a threshold temperature  $T_f$ , as evidenced e.g., by a discrepancy between field-cooled and zero-field-cooled magnetisation. The 2in-2out spin ice regime undergoes a continuous crossover to trivial paramagnetic behaviour around  $T_p$ .

An example can be found in the use of Debye-Hückel theory to obtain the low temperature heat capacity of spin ice. This is discussed in detail in Ref. [18] and we only report here a brief outline of the approach for illustrative purposes. In order to compute the heat capacity, one often looks for ways to approximate the free energy of the system. With strongly correlated localised spins, it is customary for instance to use appropriate truncated expansions. Rather than working with the spins directly, however, in spin ice one can choose to work with the effective description in terms of a gas of Coulomb interacting charges, focusing on the nature of the elementary excitations and neglecting, to a first approximation, the 2in-2out spin background. One can then assemble the free energy of the system in this new language:

$$F = F_{\text{chem pot}} + F_{\text{charge entropy}} + F_{\text{el}} \quad (1)$$

where  $F_{\text{chem pot}}$  is the contribution due to the fact that emergent excitations cost energy (chemical potential);  $F_{\text{charge entropy}}$  is the entropic contribution of distributing point charges on a lattice; and  $F_{\text{el}}$  is the electrostatic (or, better, magnetostatic) contribution.

The first two terms are straightforward.  $F_{\text{chem pot}} \propto \rho \Delta$ , where  $\rho$  is the monopole density and  $\Delta$  is their bare energy cost (i.e., their cost in a generic 2in-2out spin ice configuration infinitely far away from any other monopoles).  $F_{\text{charge entropy}} \propto -TS_{\text{mixing}}$ , where the mixing entropy takes the usual form  $S_{\text{mixing}} \propto -\rho \ln \rho - (1 - \rho) \ln(1 - \rho)$  (for a more detailed expression accounting for positive and negative charges separately, see Ref. [18]).

The third term is a tall order and an exact expression is not known. However, several analytical approximations are readily available in the literature of Coulomb liquids and charge plasmas. One of the simplest approximations goes under the name of Debye-Hückel theory (see e.g., Ref. [42]). It provides an analytical expression for  $F_{\text{el}}$  in terms of the ratio between the Coulomb interaction strength at nearest neighbour distance,  $E_{\text{nn}}$ , and temperature  $T$  as:

$$F_{\text{el}} \propto -T \left[ \frac{x^2}{2} - x + \ln(1 + x) \right], \quad x \propto \sqrt{\frac{E_{\text{nn}}}{T}} \rho \quad (2)$$

We now have an expression for the full free energy  $F$  as a function of the monopole density  $\rho$ . All the relevant parameters ( $\Delta$ ,  $E_{\text{nn}}$ ) and the proportionality constants that have been carefully omitted above can in fact be obtained independently from microscopic details about spin ice. Therefore, by minimisation with respect to  $\rho$  one can solve for the thermodynamic equilibrium value of the monopole density as a function of temperature. From the latter, one then obtains the free energy of the system and, using known thermodynamic relations, the heat capacity. In the non-interacting limit  $F_{\text{el}}$ , analytic expressions can be obtained, whereas in the Debye-Hückel case one has to resort to a recursive set of equations that can be solved numerically to the desired accuracy.

The outcome is in excellent agreement with numerical simulations as well as the experimentally measured behaviour of the heat capacity of the system at low temperature [43] – far better than one can achieve with conventional approaches for strongly interacting localised spin systems. The Debye-Hückel approach also allows to obtain further insight in the system, for instance the behaviour of the monopole density and their screening length.

***Exercise:*** using the parameters in Ref. [18], compute  $F(\rho)$  in the Debye-Hückel approximation and obtain the recursive equations for the equilibrium monopole density.

The benefit of a Coulomb liquid description is not limited to thermodynamic properties. It is also key to understand response and equilibration in these systems. A generic spin in a 2in-2out background can only flip if a thermal fluctuation allows it to overcome the energy barrier to create a monopole-antimonopole pair,  $\Delta_s = 2\Delta - E_{\text{nn}}$ . This is unlikely to happen when the temperature is appreciably smaller than the barrier, as the spin flip process takes a correspondingly long time  $\sim e^{\Delta_s/T}$ . On the contrary, three of the four spins next to an isolated monopole can flip without incurring such large energy barrier. Their reversal results in the monopole hopping from one tetrahedron to the next (see Fig. 2) whereby the number of monopoles remains unchanged (we disregard here the weaker energetic contribution due to long range interactions with possible farther monopoles).

The first process can take place at a density  $\sim (1 - \rho)$  of sites on the lattice. Therefore the associated time scale is  $\tau \sim e^{\Delta_s/T}/(1 - \rho) \sim e^{\Delta_s/T}$ , at the regime of interest of sufficiently low temperatures where  $\rho \sim e^{-\Delta/T} \ll 1$ . The second process does not incur an energy barrier but it can only take place next to an existing monopole, and therefore  $\tau \sim 1/\rho \sim e^{\Delta/T}$ . Which of the two processes dominates is determined by the smallest of the two energy scales,  $\Delta$  and  $\Delta_s = 2\Delta - E_{\text{nn}}$ . In known spin ice materials,  $\Delta > E_{\text{nn}}$  and spin flip via monopole hopping is exponentially preferred at low temperatures.

From these observations, we conclude that magnetic monopoles act as facilitators for the spin flip dynamics in the system. Therefore, they play a key role in the way the system responds to external perturbations and equilibrates. Typical time scales for macroscopic response are proportional to the inverse density of monopoles,  $\tau \sim \tau_0/\rho$ , where  $\tau_0$  is some characteristic single spin flip time scale. A hydrodynamic theory that demonstrates this relationship for non-interacting monopoles is presented in Ref. [17]. This result captures well the leading order divergence of magnetic relaxation time



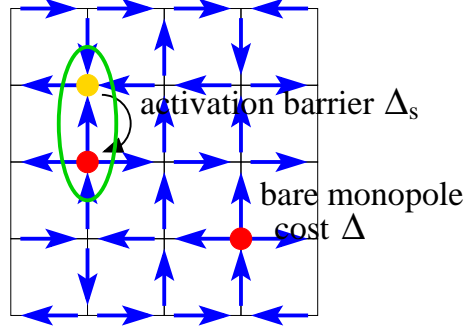


Figure 2: Left panel: a generic spin reversal in 2in-2out spin ice incurs a large energy barrier due to the creation of a monopole-antimonopole pair. Right panel: a monopole acts as a spin facilitator, in that it allows three of the four neighbouring spins to flip without such barrier. Flipping one of those spins results in the monopole hopping to a neighbouring tetrahedron and no energy change in the system.

scales observed in AC susceptibility measurements [16, 23]. Corrections due to the Coulomb interactions between monopoles were investigated numerically in Ref. [23]. (See also Refs. [25, 26, 24, 27, 28, 44, 19] for other factors playing a role in the dynamical slowing down at low temperatures, and potentially interesting open issues.)

***Suggested reading:*** see Ref. [17] for a derivation of the linear response dynamics in the non-interacting monopole approximation using hydrodynamics of irreversible processes.

In general, a system where point-like excitations freely moving in three dimensions are responsible for bulk magnetic response is bound to exhibit an interesting separation of time scales. On the one hand, monopoles are only created and annihilated in pairs. Therefore, monopole density relaxation processes involve monopole motion over distances of the order of the average monopole-monopole separation,  $\xi \sim \rho^{-1/3}$ . In a ballistic regime where positive monopoles are driven towards negative monopoles, the corresponding time scale is of the order of  $\xi$  monopole hops. At sufficiently high temperatures and / or beyond the screening length, the monopole motion is diffusive and the time scales as  $\xi^2 \sim \rho^{-2/3}$ . Finally, any changes in the bulk magnetisation and other observables that depend on the local spin orientations require the monopoles to visit a finite fraction of the spins in the systems. Therefore on average they have to move across a finite fraction of  $\xi^3$  spins per monopole, corresponding to a time scale of the order of  $\xi^3 \sim \rho^{-1}$ .

The Coulomb liquid nature of low-temperature excitations leads to other unusual features in the dynamical behaviour of driven spin ice systems close to equilibrium. For example, response properties typical of electrolytes have been argued to apply to spin ice, e.g., in the form of an increase in the monopole density upon switching on an external magnetic field, the analogue of the second *Wien effect* [30, 13, 29] in electrolytes. Experimental work testing this hypothesis was presented [13] but no consensus has been reached yet on the observation of a magnetic Wien effect.

**Suggested reading:** *it is insightful to revisit Onsager’s theory for electrolytes (see e.g., Ref. [29]) and translate it into the magnetic language appropriate for spin ice [13].*

These examples illustrate the close interplay between the nature of the fractionalised excitations in spin ice and its dynamical properties. Such interplay is bound to be reflected if not enhanced when the system is brought strongly out of equilibrium. In the following, we shall discuss a couple of examples in some detail. Specifically, we shall consider sudden quenches from a high to a low monopole density state, triggered by either tuning the temperature or an applied magnetic field.

We mention in passing that the phase diagram of spin ice includes a critical end point in presence of a magnetic field. “Slow quenches” (i.e., continuous variations of the parameters as a function of time) to / across the critical point should therefore give rise to out-of-equilibrium scaling behaviour à la Kibble-Zurek, in the novel context of a system with emergent gauge symmetry and emergent Coulomb-interacting quasiparticles. Theoretical work investigating this possibility is currently under way.

## 2.1 Thermal quenches

One way to cause the system to evolve from a state with high monopole density to a state with low monopole density is by lowering its temperature. Here we consider for simplicity the case where the system is initially at infinite temperature (Ising paramagnet) and it is suddenly quenched to a target (low) temperature [31]. In effective Coulomb liquid terms, this is equivalent to quenching a plasma where positive and negative charges can be created (and annihilated) only in pairs, and each charge costs some finite amount of energy  $\Delta$ .

Immediately after the quench, the system is strongly out of equilibrium (e.g., the monopole density is much larger than its thermodynamic value at the target temperature). When coupled to a thermal bath, it will relax to equilibrium via the available dynamical processes, namely monopole motion and monopole-antimonopole creation/annihilation.

Note the stark contrast with conventional magnets where thermal quenches are usually described in terms of domain nucleation, growth and coarsening [32]. In spin ice, it is clear that this language is unlikely the right one to understand the evolution of the system. Rather, we see that the language of reaction-diffusion processes is more befitting.

Whereas, monopole-antimonopole annihilation events lower the energy of the system, pair creation events face a finite energy cost  $\Delta_s$ . Detailed balance (i.e., the requirement that the dynamical processes are compatible with thermodynamic equilibrium) imposes that creation is statistically suppressed with respect to annihilation by a Boltzmann factor  $\exp(-\Delta_s/T)$ .

For the sake of the discussion below, we limit ourselves to the case where the target temperature is much smaller than the pair creation energy cost and  $\exp(-\Delta_s/T) \sim 0$ . We can thus neglect creation processes altogether. Within this assumption, the equilibrium density of monopoles at the target temperature is also vanishingly small and we shall set it to zero (recall that  $\rho \sim e^{-\Delta/T}$  and  $\Delta < \Delta_s < 2\Delta$ , therefore

$\Delta_s \gg T$  implies  $\Delta \gg T$  and  $\rho \sim 0$ ). The equations of motion for the monopole density can be generically written as [15]:

$$\begin{aligned} \frac{\partial \rho_{\pm}(r, t)}{\partial t} + \nabla \cdot \mathbf{J}_{\pm} &= -\kappa \rho_{+}(r, t) \rho_{-}(r, t) \\ \mathbf{J}_{\pm} &= -D \nabla \rho_{\pm}(r, t) - \mu q_{\pm} \rho_{\pm}(r, t) \nabla V(r, t) \end{aligned}$$

where  $\rho_{\pm}$  and  $\mathbf{J}_{\pm}$  are the densities and currents of positive and negative monopoles, respectively,  $\kappa$  is the annihilation reaction constant, and the two current terms are due to diffusion (constant  $D$ ) and deterministic drift caused by (long range) interactions (mobility  $\mu$ , interaction potential  $V(r)$ ). In spin ice systems, it is often the case that the relevant constants can be estimated analytical or obtained from independent comparison to simulations / experiments, remarkably leaving few to no fitting parameters in the equations!

### 2.1.1 Nearest-neighbour spin ice

Let us focus firstly on the case where spin-spin interactions are truncated at nearest-neighbour distance and correspondingly the charges in the Coulomb liquid language are non-interacting ( $V(r) = 0$ ). Incidentally, in this case  $\Delta_s = 2\Delta$ .

Within these approximations, the dynamical processes in the system are limited to diffusion of non-interacting charges and monopole-antimonopole annihilation events. At mean field level (uniform system, no spatial dependence), the diffusive part is irrelevant and we are left with a straightforward reaction equation:

$$\frac{d\rho}{dt} = -\kappa \rho^2(t). \quad (3)$$

The right hand side is determined by the rate of monopole annihilation events, which is proportional to the probability of finding a monopole-antimonopole pair in the system ( $\sim \rho^2$ ) divided by the characteristic time scale for a single annihilation event to take place (namely, the characteristic spin flip time scale  $\tau_0$ ). The constant  $\kappa \propto 1/\tau_0$  depends on details of the underlying microscopic lattice through a combinatorial factor accounting for the ways to arrange two monopoles next to one another across a bond of the lattice.

**Exercise:** provide an estimate of  $\kappa$  for spin ice on the pyrochlore lattice and compare your answer with the two values provided in Ref. [31] and reported in the caption of Fig. 3.

The mean field Eq. (3), complemented by the initial condition  $\rho(t = 0) = \rho_0$ , can be solved straightforwardly to find

$$\rho(t) = \frac{\rho_0}{1 + \kappa \rho_0 t} \quad (4)$$

and the long time decay in the monopole density goes as  $t^{-1}$ . The accuracy of the mean field solution in describing the behaviour of nearest-neighbour spin ice depends crucially on how uniform the initial charge distribution is, to ensure that diffusion time scales are indeed irrelevant.

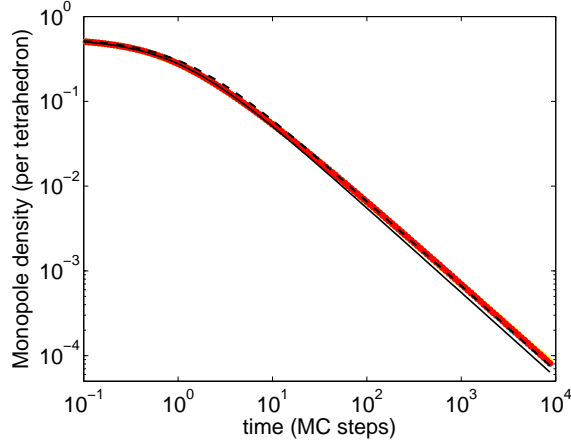


Figure 3: Monopole density evolution in nearest neighbour spin ice, after a thermal quench from  $T = 10$  K to  $T = 0$  K, for system sizes  $L = 32, 64, 128$ . The analytical mean-field result Eq. (4) is shown for  $\kappa = 3/2\tau_0$  (dashed black line) and  $\kappa = 9/5\tau_0$  (solid black line) – see Ref. [31].

Spatial variations in the initial distribution of monopoles and antimonopoles can however alter the behaviour significantly [14]. For instance, if the charges are distributed entirely at random with density  $\rho_0$ , then the net charge fluctuations in a volume of linear size  $\ell$  scale as  $\sqrt{\rho_0 \ell^3}$ . Given that annihilation processes conserve the local net charge (they always remove one positive and one negative monopole), they cannot remove these fluctuations. After a time  $t$  sufficient for monopoles to diffuse over the length  $\ell$  (i.e.,  $\ell = \sqrt{Dt}$ ), all possible annihilation events within the volume of size  $\ell$  will have taken place, leaving behind a number  $\sim \sqrt{\rho_0 \ell^3}$  of monopoles of the same charge due to the statistical net charge fluctuation. The density of leftover monopoles scales as  $\sqrt{\rho_0 \ell^3} / \ell^3 = \rho_0^{1/2} (Dt)^{-3/4}$ ; it decays with time more slowly than the mean field behaviour ( $\sim t^{-1}$ ) and therefore dominates at long times. (We refer the reader to Ref. [14] for a more detailed derivation and discussion of this result.)

However, none of this in fact applies to spin ice. As a monopole travels along a given path across the system, it modified the underlying spin ice vacuum by polarising the spins along the path. Another monopole of the same charge *cannot* follow the same path in the same direction. Equivalently, we can at most drive  $\ell^2$  monopoles of equal charge across a system of linear size  $\ell^3$  before the system becomes fully polarised and no more monopoles of the same charge can travel in that same direction. This means that the most net charge that can accumulate in a volume  $\ell^3$  of a spin ice system is of the order  $\ell^2$ . The density of leftover monopoles in spin ice therefore scales as  $\sqrt{\ell^2} / \ell^3 = (Dt)^{-1}$  rather than  $(Dt)^{-3/4}$ , which is no longer asymptotically slower than mean field behaviour.

These observations are confirmed by the excellent agreement between Monte Carlo simulations of thermal quenches in nearest neighbour spin ice and the solution of the

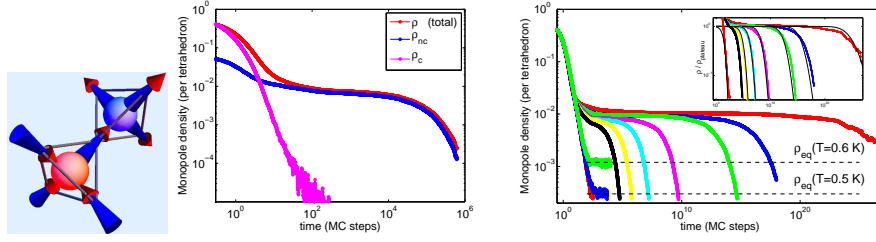


Figure 4: Left panel: Spin configuration of two adjacent tetrahedra hosting a non-contractible monopole-antimonopole pair. Middle panel: Monte Carlo simulation of dipolar spin ice, showing the total monopole density (red), noncontractible pair density (blue), and free monopole density (magenta), following a thermal quench from  $T = \infty$  to  $T = 0.125$  K, with system size  $L = 8$  and  $\text{Dy}_2\text{Ti}_2\text{O}_7$  parameters. Right panel: Decay of the total monopole density in Monte Carlo simulations of dipolar spin ice, following thermal quenches from infinite temperature to different finite target temperatures (see Fig.3 in Ref. [31] for details). Inset: comparison of the long time tail of the monopole density to the Poissonian modelling of the spontaneous decay of noncontractible pairs discussed in the text.

mean field equation, Eq. (4), illustrated in Fig. 3. Notice that the agreement is achieved without any fitting parameters!

### 2.1.2 Dipolar spin ice

Let us then consider the case of dipolar spin ice, where monopole excitations are coupled by long range Coulomb interactions. In general, they introduce an additional energetic term that has a smoothing effect on spatial fluctuations of the net charge. Therefore, the naive expectation from this coarse grained picture is that the monopole density decay following a thermal quench in dipolar spin ice is at least as fast as the nearest neighbour case. (We refer the reader to Ref. [15] for a discussion of annihilation-diffusion reaction processes with long-range interactions.)

Monte Carlo simulations confirm this expectation at short times, as illustrated in Fig. 4, right panel. However, for sufficiently low target temperatures, a long-lived metastable plateau develops in the time evolution of the monopole density. This new and unexpected feature is due to a curious interplay between long-range emergent physics (the Coulomb liquid description) and lattice-scale physics (related to how monopole motion changes the underlying spin ice vacuum).

When a positive and a negative monopole meet in spin ice, the spin between them can sometimes be the minority spin rather than one of the three majority ones, as illustrated in Fig. 4, left panel. In this case, flipping the spin does not annihilate the two monopoles but rather creates an even more energetically costly defect: a 4in and a 4out pair of tetrahedra. At low temperatures, the likelihood of such process is so low that it is effectively forbidden. We shall dub them *noncontractible* monopole pairs. Once they meet at the ‘wrong’ spin (i.e., the minority spin), the two monopoles of a noncontractible pair are bound together, held by their reciprocal Coulomb attraction. This is a

direct consequence of the long-range nature of the dipole-dipole interaction.

The monopoles forming noncontractible pairs do not need necessarily to separate in order to be able to annihilate. It can also happen that another (free) monopole collides with the pair, whereby it can annihilate one of the monopoles in the pair (that with opposite charge to the free monopole) and free up the other one. Pictorially, one can think of this as *radioactive decay*, triggered by the absorption of a monopole, in contrast to *spontaneous decay* of the pair, where the monopole and antimonopole separate and annihilate elsewhere on the lattice. The radioactive process straightforwardly reduced the energy of the system whereas the spontaneous process incurs a finite energy barrier.

Which of the two processes controls the long time decay of the monopole density depends on the relative population of free monopoles and noncontractible pairs. If free monopoles are abundant, then nearly all noncontractible pairs decay radioactively (vanishing energy barrier, fast relaxation channel). If instead most monopoles in the system form noncontractible pairs, then their annihilation must occur via spontaneous decay (slow relaxation channel, due to the finite activation energy barrier).

At high-temperature, when the system is nearly paramagnetic and the defects are dense, one can readily verify that the density of free monopoles is statistically larger (by about one order of magnitude) than the density of noncontractible pairs – as reflected in the initial conditions that can be inferred from Fig. 4, right panel. Therefore, we see that a *population inversion* is required to cause the system to relax via the slow channel and to develop a long-lived metastable plateau at low temperature.

***Exercise:*** obtain an estimate of the density of noncontractible pairs in the paramagnetic limit (i.e., randomly oriented Ising spins), and compare it to the total density of monopoles in the same state.

Once again, the long range Coulomb interaction plays a crucial role in determining how the free vs noncontractible monopoles evolve with time. Indeed, free monopoles and antimonopoles are drawn together by Coulomb forces which are stronger than the attraction between free monopoles and noncontractible pairs (charge-dipole interaction). Naively, one would thus expect that the long range interactions favour direct annihilation of free monopoles over the radioactive decay of noncontractible pairs. If the bias is sufficiently pronounced, it can eventually cause the density of free monopoles to become vanishingly small, whereas the density of noncontractible pairs remains finite, leading to the above mentioned population inversion.

Numerical Monte Carlo simulations of dipolar spin ice suggest that this understanding of the behaviour of the system in terms of a Coulomb liquid picture of monopoles and noncontractible pairs is in fact correct. In particular, the population inversion does take place and the density of noncontractible pairs is solely responsible for the long lived metastable plateau (see middle panel in Fig. 4).

As in the case of nearest-neighbour spin ice, one can use differential equations for reaction-diffusion processes to model the evolution of the monopole density following a quench and to confirm the qualitative understanding presented above. The processes that ought to be included are:

1. monopole-antimonopole annihilation
2. noncontractible pair formation

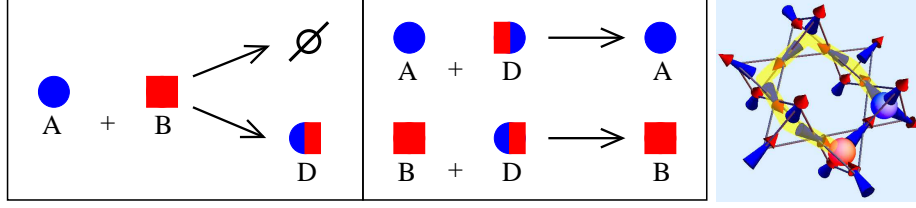


Figure 5: Left panel: Qualitative illustration of the dynamical processes involved in the monopole density evolution following a thermal quench in dipolar spin ice. (A=positive and B=negative monopole; D=noncontractible pair). Right panel: Example of a hexagonal path for the spontaneous decay of a noncontractible pair.

### 3. radioactive and spontaneous decay of noncontractible pairs.

They are qualitatively illustrated (with the exception of the spontaneous decay) in the left panel of Fig. 5. In contrast to the nearest neighbour case, one has to introduce an additional density variable to represent noncontractible pairs (a new ‘species’ of particles whose evolution is directly related to that of the free monopoles).

**Exercise:** write the differential equations corresponding to the diagrams in Fig. 5, left panel, in the mean field limit. Consider explicitly the limit where temperature is much smaller than the energy barrier for spontaneous decay and noncontractible pairs can only decay radioactively. Solve the equations either analytically or numerically and compare the free vs noncontractible monopole densities (you should use initial conditions similar to those in the middle panel of Fig. 4). Try to identify qualitatively the range of parameters in the differential equations for which a population inversion takes place and comment whether spin ice is likely to fall within this range or not. (The differential equations coefficients for spin ice can be estimated from microscopic probabilistic arguments akin to the derivation of  $\kappa$  in the nearest neighbour case.)

Here we limit ourselves to modelling in some detail the long time tail of the monopole density decay. As discussed above, it is evident from the middle panel of Fig. 4 that the noncontractible pairs are largely responsible for this tail. Moreover, in this regime we expect that spontaneous decay of noncontractible pairs is the leading dynamical process in the system.

Firstly, we ought to estimate the typical energy barrier  $\Delta E_{nc}$  of a spontaneous decay process. This is determined by the largest distance that a monopole and an antimonopole in a noncontractible pair need to be separated by before they are able to annihilate elsewhere in the lattice. The shortest possible path is illustrated in the right panel of Fig. 5. It requires separating the two monopoles up to third neighbour distance, before they are brought together again to annihilate. From the value of the magnetic charge of a spin ice monopole, using the known lattice spacing and the formula for the magnetic Coulomb interaction, one can readily obtain

$$\Delta E_{nc} = -\frac{\mu_0}{4\pi} Q_m^2 \left( \frac{1}{d_{3n}} - \frac{1}{d_{nn}} \right).$$



**Exercise:** using spin ice parameters in the literature, compute the value of  $\Delta E_{\text{nc}}$  for  $\text{Dy}_2\text{Ti}_2\text{O}_7$  and  $\text{Ho}_2\text{Ti}_2\text{O}_7$ .

Now that we have an estimate of the energy barrier, we can proceed with modelling the spontaneous decay of noncontractible pairs. (Notice that the existence of a hexagonal decay path for each noncontractible pair is far from obvious and ought to be regarded as a working assumption here; it will be confirmed a posteriori by comparison with simulations.) We shall assume that the spontaneous decay events are uncorrelated and they obey a Poissonian distribution, with decay probability per unit time  $\mathcal{P}(t) = e^{-t/\tau_{\text{nc}}}/\tau_{\text{nc}}$ . The time scale for the activated process is  $\tau_{\text{nc}} = \tau_0 e^{\Delta E_{\text{nc}}/T}$ , where  $\tau_0$  is the characteristic microscopic spin flip time scale ( $\tau_0 = 1$  in Monte Carlo simulations). Finally, the noncontractible pair density at time  $t$  is determined by the number of pairs that have not annihilated via spontaneous decay at any  $t' \leq t$ , i.e.,

$$\rho(t) \propto 1 - \int_0^t \mathcal{P}(t') dt' \propto e^{-t/\tau_{\text{nc}}}. \quad (5)$$

In the Coulomb liquid description, the value of  $\Delta E_{\text{nc}}$  is well-defined. However, one should recall that it is in fact the result of a resummation of the dipolar interactions between spins which neglects quadrupolar corrections [12]. Therefore, it is subject to (small) statistical fluctuations in Monte Carlo simulations of dipolar spin ice, which are reasonably fitted by a Gaussian distribution. In the case of  $\text{Dy}_2\text{Ti}_2\text{O}_7$  for example, the peak of the distribution occurs at  $\Delta E_{\text{nc}} \simeq 1.47$  K and the variance is  $0.01$  K<sup>2</sup> [31]. The value of  $\rho(t)$  in Eq. (5) ought to be averaged over such Gaussian distribution before comparing with simulations:

$$\mathcal{G}(\Delta E) \propto \exp \left[ -\frac{(\Delta E - \Delta E_{\text{nc}})^2}{2\sigma^2} \right] \quad (6)$$

$$\begin{aligned} \langle \rho(t) \rangle_{\text{dis}} &\propto \int \mathcal{G}(\Delta E) \rho(t; \Delta E) d\Delta E \\ &\propto \int \exp \left[ -\frac{(\Delta E - \Delta E_{\text{nc}})^2}{2\sigma^2} \right] \exp \left[ -\frac{t}{\tau_0 e^{\Delta E/T}} \right] d\Delta E. \end{aligned} \quad (7)$$

Notice that Eq. (5) has only one fitting parameter left: the proportionality constant, i.e., the height of the metastable plateau induced by the long-lived noncontractible pairs. The comparison between theory and simulations is illustrated in the inset of the right panel in Fig. 4. We note the good agreement over *more than 20 orders of magnitude*(!), demonstrating that the qualitative understanding in terms of Coulomb liquid and noncontractible pairs is indeed correct, and that the choice of single-hexagon paths for the spontaneous decay is justified.

We close by stressing the role played by the long range Coulomb interactions between the monopoles in determining the strikingly different behaviour in dipolar vs nearest neighbour spin ice. On the one hand, they are responsible (at short range) for the existence of metastable noncontractible pairs. On the other hand, their long range nature contributes to the population inversion that is key to the long time plateau in the monopole density at low temperatures.

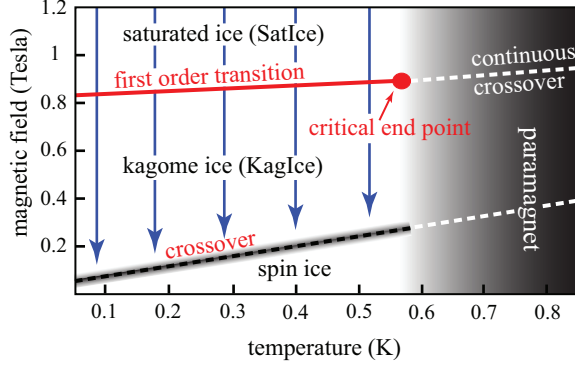


Figure 6: Phase diagram of spin ice in presence of a  $[111]$  field. The vertical arrows represent field quenches from saturated ice (high monopole density) to kagome ice (low monopole density), discussed in the text.

## 2.2 Field quenches

An alternative protocol to drive a spin ice system from high to low monopole density involves the use of an applied magnetic field pointing in one of the global  $[111]$  crystallographic directions. For intermediate and large field strength, the field maps in the Coulomb liquid language onto a (staggered) chemical potential for the monopoles [12]. The resulting phase diagram is that which is typical of a liquid-gas system, with a first order transition line ending at a critical end point (see Fig. 6).

To understand this phase diagram, it is convenient to divide the spin lattice (pyrochlore, or corner-sharing tetrahedral lattice) into alternating kagome and triangular layers perpendicular to the field direction, as illustrated in Fig. 7, left panel. In the limit of strong fields (the saturated ice regime), all of the spins point along the field direction while respecting the local easy axes (Fig. 7, middle panel). The ice rules are violated everywhere and each tetrahedron hosts a monopole; the monopoles form an ‘ionic crystal’ of alternating positive and negative charges. As the field strength is reduced, violations of the ice rules are no longer sufficiently offset by a gain in Zeeman energy and a regime where most tetrahedra obey the ice rule is recovered (at low temperature). This necessarily requires some of the spins to point against the applied field. At intermediate field strengths, these are mostly spins in the kagome planes, because their Zeeman energy is smaller by a factor of three compared with the spins in the triangular planes. This leads to an extensively degenerate regime known as kagome ice, illustrated in Fig. 7, right panel. At low field strengths, the kagome ice regime becomes entropically unstable to the conventional spin ice regime, namely the ensemble of all configurations satisfying the ice rules irrespective of the polarisation of the triangular spins. All of these regimes cross over at sufficiently large temperatures into a conventional paramagnetic regime.

The range of behaviours that can be investigated in quenches involving an applied field is far richer than in thermal quenches [33]. For instance, the presence of phase transitions can lead to qualitatively different responses, including the possibility of crit-

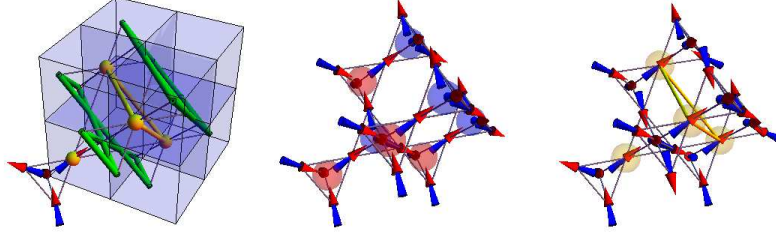


Figure 7: Left panel: With respect to the global  $[111]$  direction identified by the field, the pyrochlore lattice can be seen as a stack of triangular (yellow) and kagome (green) layers perpendicular to the field direction. The easy axis of the triangular spins is parallel to the field whereas the kagome easy-axes are canted, all with the same projection factor  $1/3$  onto the field direction. Middle panel: Saturated spin ice state. Right panel: An example of a kagome ice spin configuration.

ical slowing down and universal scaling à la Kibble-Zurek. The fact that triangular and kagome spins couple differently to the applied field can be used to tune the dimensionality of the system ( $2D \leftrightarrow 3D$ ). Moreover, the ability to tune both temperature and Zeeman energy against the long range Coulomb interaction allows to control the dynamical processes at play and even to alter the characteristic monopole hopping time scales.

Here we focus for simplicity on field quenches across the first order transition, while the temperature is held constant. Our initial condition is the large field (saturated ice) state, where each spin has positive projection in the direction of the field (Fig. 7, middle panel). Every ‘upward pointing’ tetrahedron is occupied by a positive monopole and every ‘downward pointing’ tetrahedron is occupied by a negative monopole. Further, we only consider temperatures and target field values whereby the thermal equilibrium state after the quench is that of kagome ice. Here the Zeeman energy of the triangular spins is sufficiently larger than the temperature that they remain effectively fully polarised in the field direction. On the other hand, the Zeeman energy of the kagome spins is comparable to the temperature, and they are therefore disordered (in so far as the ice rules due to exchange and dipolar interactions allow). We note that this choice of temperature and field after the quench typically corresponds to a negligibly small equilibrium monopole density – hence the quenches can be regarded once again to be from high to zero monopole density, albeit the starting configuration is much different from the initial paramagnetic state used in thermal quenches. For a more detailed discussion of  $[111]$  field quenches in spin ice, we refer the reader to Ref. [33].

### 2.2.1 Initial decay

Immediately following a field quench from saturated ice at low temperature, the monopole density is far greater than its thermodynamic equilibrium value. Therefore, dynamical

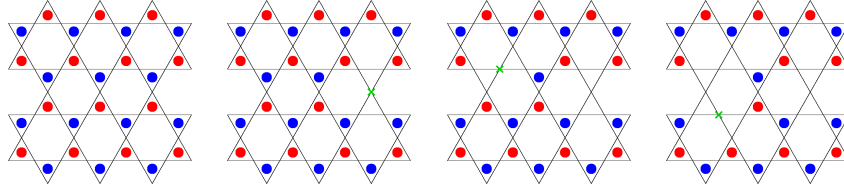


Figure 8: Pictorial representation of the initial monopole annihilation processes within a kagome plane, from left to right. Positive and negative monopoles are represented by red and blue dots; the spins are not shown for simplicity. The green crosses indicate the spins the have flipped in going from one configuration to the next (left to right panels).

spin flip processes that lead to monopole-antimonopole annihilation become favoured.

Notice that the triangular spins do not participate in the initial decay of the monopole density. Not only they are pinned by a larger Zeeman energy than the kagome spins, but also – and more importantly – they are akin to the intervening spin in a noncontractible pair. Flipping a triangular spin in saturated ice leads to the creation of a 4in and a 4out defect rather than to the annihilation of two monopoles.

The initial dynamics of a field quench is thus confined to the 2D kagome planes. Here, flipping a spin between two monopoles leads to their straightforward annihilation, which lowers the energy of the system. The process continues so long as there are kagome spins available, akin to a random dimer deposition process on the bonds of the dual honeycomb lattice (see Fig. 8).

Notice that dimers can sometimes ‘desorb’ during the initial decay when thermal fluctuations lead to a second reversal of the same spin, thus creating anew the two monopoles that had been previously annihilated. The desorption rate can be controlled by tuning the value of the target field as well as the temperature. Here we focus for simplicity on the regime where the desorption rate is negligible.

Ignoring the long-ranged Coulomb interaction between the monopoles, one should expect to be able to model the initial decay process with reasonable accuracy at the mean field level, given the uniformity of the charge distribution in the initial (saturated) state. The equation of motion is thus the same as for nearest-neighbour thermal quenches, Eq. (3). The agreement with Monte Carlo simulations of field quenches in dipolar spin ice is excellent without fitting parameters (Fig. 9), suggesting that the Coulomb interactions do not have a measurable effect on the reaction process.

The solution of the mean field equations is temperature independent. As time passes, we see from Fig. 9 that the results of the simulations eventually depart from the mean field behaviour and become strongly temperature dependent. This signals the end of the initial (dimer deposition like) regime. Randomly selected neighbouring monopoles have straightforwardly annihilated until only isolated ones are left behind and they need to diffuse across the system before their density can decay further.

**Exercise:** implement a numerical algorithm (e.g., Monte Carlo) to estimate the density of leftover monomers following a dimer deposition process on the honeycomb lattice. Compare it with the density of monopoles in dipolar spin ice simulations at the end of the initial decay (from Fig. 9). Comment on the comparison in light of the

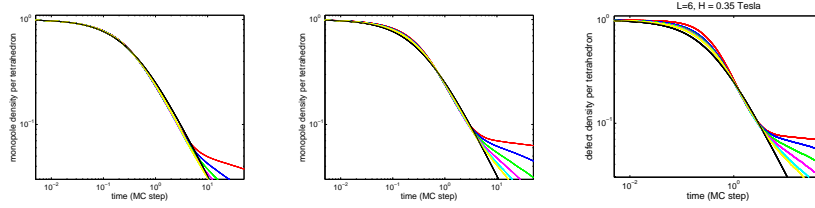


Figure 9: Monte Carlo simulations of field quenches in dipolar spin ice for different values of the target field ( $H = 0.2, 0.3, 0.35$  Tesla, from left to right). Only the initial (short time) decay of the monopole density is shown. The different colour curves correspond to different values of the temperature and the superposed black line is the solution of the mean field equation Eq. (3), without any fitting parameters.

*fact that spin ice simulations include small but non-zero desorption probability and long-range Coulomb interactions.*

When the target field value becomes sufficiently large, it is no longer possible to disregard desorption events. This is the likely cause of the departure from mean field behaviour at short times, which begins to appear in the right panel of Fig. 9.

### 2.2.2 Intermediate regime

The initial decay ends when there are no more monopole and antimonopoles next to one another that can be annihilated by flipping the intervening spin. Monopoles are now required to travel across the lattice before their density can be further reduced.

Fig. 10 illustrates the behaviour over a large time window, for different fields and temperatures. In general, we observe that the relaxation time scales in the system become substantially longer after the initial decay discussed in the previous section. The new time scales show a clear temperature dependence (the lower the temperature, the slower the decay), as one would expect in presence of activation energy barriers obstructing the relaxation. This scenario is similar to the one observed in thermal quenches in dipolar spin ice (Fig. 4, right panel). However, we see that the behaviour in field quenches is far richer, with intermediate time regimes that appear to be distinct from both the initial as well as the asymptotically long time decay.

These intermediate regimes are controlled by finite size, finite time processes and are rather challenging to model analytically. The comparison between analytics and numerics is not as straightforward when we do not have access to some asymptotic limit (e.g., short or long times). This interesting and unique regime of an emergent reaction-diffusion process in presence of long-range Coulomb interactions and kinematic constraints, which can in principle be accessed experimentally in spin ice materials, lacks indeed a proper understanding to date.

### 2.2.3 Long time behaviour

At long times, the monopole density decay becomes increasingly dominated by the longest relaxation time scale in the system. We should therefore be able to capture the

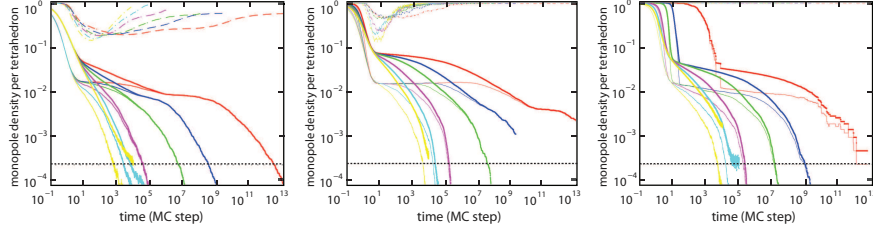


Figure 10: Monopole density (thick lines), density of triangular spins in the direction of the initial magnetisation (thin dotted-dashed lines), and density of noncontractible pairs (thin solid lines) from MC simulations for a system of size  $L = 8$  (8192 spins), fields  $H = 0.2, 0.4$ , and  $0.6$  Tesla (from left to right panels), and temperatures  $T = 0.1, 0.15, 0.2, 0.3, 0.4$ , and  $0.5$  K (red, blue, green, magenta, cyan, and yellow, respectively). At intermediate times, some of the triangular spins reverse, as shown by the dip in their density; the latter has been magnified by a factor of 100 and 1,000 (left and centre panels, respectively) for visualisation purposes. In the right panel, the density of triangular spins in the direction of the applied field remains very nearly 1 throughout the simulations; the triangular spins remain polarised throughout the quench and the monopole motion is effectively 2D. (The black dotted horizontal line in each figure indicates the density threshold of one monopole in the entire MC system.)

physics of this regime by modelling analytically its asymptotic behaviour.

Whereas at small and intermediate target field values (left and middle panels in Fig. 10) most of the monopoles at long times form noncontractible pairs, this is clearly not the case at larger fields (right panel in Fig. 10). Hereafter, we shall focus for simplicity only on the latter case.

For large field values, the long relaxation times cannot be ascribed to long-lived noncontractible pairs. Rather, it must be that an energy barrier impedes the diffusion and annihilation of free monopoles. The origin of this barrier can be understood if we recall that monopole diffusion at large fields and low temperatures takes place nearly exclusively within each kagome plane, whilst the triangular spins remain fully polarised (Fig. 10, right panel).

Under these conditions, a positive monopole in a kagome plane has lower Zeeman energy when it sits in an upward-pointing tetrahedron than in a downward pointing tetrahedron (vice versa for a negative monopole, as illustrated in Fig. 11). If we were to make a monopole hop across the kagome lattice, at every other step it would have to overcome a Zeeman energy barrier  $dE \simeq 4.48 H K$  (where  $H$  is the value of the target field measured in Tesla).

Alternatively, the system can create a monopole-antimonopole pair next to the existing monopole and then annihilate the existing monopole with the oppositely charged member of the pair. The outcome is equivalent to moving a monopole from one Zeeman-favoured tetrahedron to another Zeeman-favoured tetrahedron two lattice spacings away from the first. This process costs interaction energy (monopole pair creation + Coulomb interactions) but it can be done while gaining Zeeman energy. The cor-

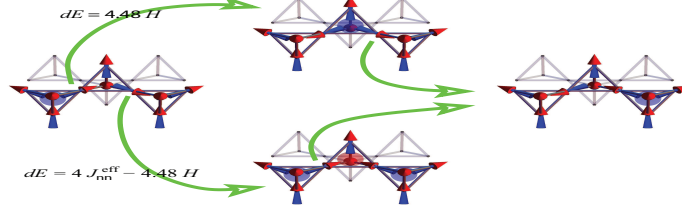


Figure 11: Schematic representation of monopole motion in a kagome plane, via ordinary hopping (upper intermediate diagram) and via pair-assisted hopping (lower intermediate diagram). Both processes result in a negative monopole being transferred from a downward-pointing tetrahedron (left diagram) to one of the four nearest downward-pointing tetrahedra (right diagram). Each process encompasses two spin flips but, according to the order in which they are executed, the two processes face different energy barriers  $dE$  with opposite field dependence. The figure shows the value of the barriers for nearest-neighbour spin ice. In the main text we discuss how they are modified in presence of long-range dipolar interactions. The field dependence, however, remains unchanged. The tails of the green arrows originate from the spin being flipped in going from one panel to the next. Only the spins in the front three tetrahedra are drawn for convenience. The triangular spins remain polarised throughout.

responding barrier, using the Coulomb liquid description, can be estimated as  $dE \simeq 2\Delta - 2E_{nn} + E_{2n} - 4.48 H$  K, where  $\Delta$  is the bare monopole cost and  $E_{nn}$  ( $E_{2n}$ ) is the strength of the Coulomb interaction between two nearest neighbour (next nearest neighbour) monopoles.

**Exercise:** using spin ice parameters for  $\text{Dy}_2\text{Ti}_2\text{O}_7$  and  $\text{Ho}_2\text{Ti}_2\text{O}_7$  from the literature, estimate the corresponding values of the pair-assisted hopping barrier.

Notice that the two dynamical processes have opposite dependence on the applied field strength. Using spin ice parameters appropriate for  $\text{Dy}_2\text{Ti}_2\text{O}_7$ , the second process (pair assisted hopping) becomes energetically favoured with respect to the first one for  $H \gtrsim 0.5$  Tesla. When  $H = 0.6$  Tesla (right panel in Fig. 10), the barrier to pair assisted hopping is of the order of 2 K whereas the barrier to ordinary hopping is approximately 3 K.

In order to confirm our understanding of the slowing down of the monopole hopping, we attempt to collapse the long time tails of the Monte Carlo simulations of dipolar spin ice by rescaling time using the characteristic activated time scale  $e^{dE/T}$ . For the target field  $H = 0.6$  Tesla, we find a good collapse when we choose  $dE = 2.4$  K, in reasonable agreement with the estimated value for the pair assisted hopping (Fig. 12). However, larger system sizes and longer simulation times are required for a more discerning and conclusive comparison [33].

In summary, field quenches in spin ice offer a realisation of several paradigmatic



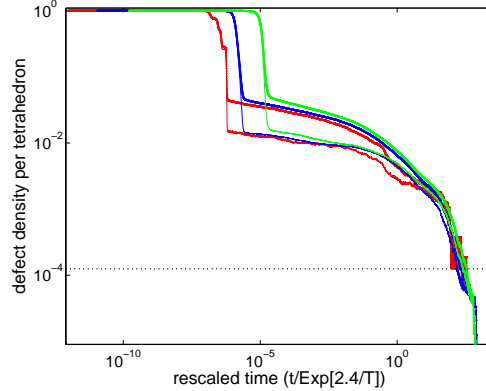


Figure 12: Collapse of the long-time decay of the monopole density (thick lines) and of the noncontractible monopole density (thin lines) after rescaling the time axis by a factor  $\exp(-2.4/T)$ . The MC simulations are for  $L = 10$  with  $H = 0.6$  Tesla and  $T = 0.13, 0.15$ , and  $0.18$  K (red, blue, and green curves, respectively). The good quality of the collapse indicates that the simulated systems are large enough for the energy scale of  $2.4$  K not to exhibit appreciable system size dependence.

concepts in nonequilibrium dynamics: dimer adsorption, Coulombic reaction-diffusion physics, and kinetically constrained slow dynamics. There is an unusually high degree of tunability, as one is able to control, say, the time scale of the elementary dynamical move through a Zeeman energy barrier; or the dimensionality of the final state ( $d = 2$  kagome vs.  $d = 3$  spin ice); or else the relative importance of dimer desorption compared with Coulomb interactions between the monomers.

Given the availability of a range of experimental probes for magnetic systems and the ability to apply time dependent fields of the strength required for spin ice materials, one can expect that it will be possible to study some of these out of equilibrium phenomena experimentally in the near future.

Further reading on recent experimental work in this direction – including a curious interplay between magnetic and thermal degrees of freedom leading to magnetic deflagration effects [45] – can be found in these papers [24, 46, 47], and references therein.

### 3 Example 2: Kitaev’s toric code

So far we considered out of equilibrium phenomena in classical topologically ordered systems. The observed interplay between the non-local nature of the phase, the emergent excitations, and local kinematic constraints is likely to give rise to interesting properties and phenomena also in related quantum mechanical systems. However, the study of strongly correlated quantum systems in two or higher dimensions far from equilibrium is in general a tall order. For this reason, we shall focus here on one of the

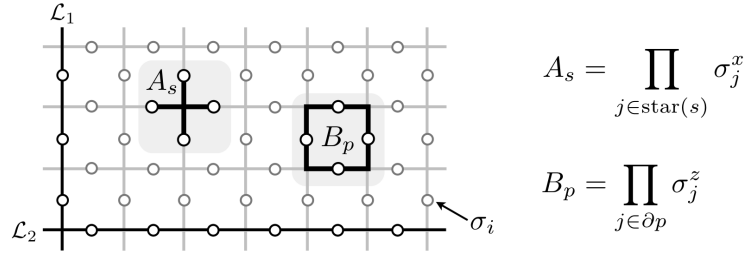


Figure 13: Illustration of the star  $A_s$  and plaquette  $B_p$  operators in the toric code Hamiltonian. The figure also shows the support of two winding loop operators on the direct lattice,  $\mathcal{L}_1$  and  $\mathcal{L}_2$  (periodic boundary conditions are assumed).

simplest examples of quantum systems that exhibit topological order in 2D: Kitaev's toric code [8].

### 3.1 The model

The toric code is a system of spin-1/2 degrees of freedom living on the bonds of a square lattice, subject to the Hamiltonian

$$H = -\lambda_A \sum_s A_s - \lambda_B \sum_p B_p, \quad (8)$$

where  $\lambda_A, \lambda_B > 0$  are two coupling constants and the star and plaquette operators  $A_s = \prod_{i \in s} \sigma_i^x$  and  $B_p = \prod_{i \in p} \sigma_i^z$  are defined as in Fig. 13. (The experienced reader will recognise this as a gauge-fixed lattice gauge theory.) The beauty of the model lies in its simplicity. Every term in the Hamiltonian commutes with every other, namely  $[A_s, A_{s'}] = 0$ ,  $[B_p, B_{p'}] = 0$ , and  $[A_s, B_p] = 0$ , for all  $s, s', p, p'$ . One can therefore diagonalise simultaneously all these operators. Every eigenstate of  $H$  is also an eigenstate of each  $A_s$  and  $B_p$  (which have eigenvalue  $\pm 1$ ). With the choice of  $\lambda_A$  and  $\lambda_B$  both positive, the ground state  $|\psi_0\rangle$  satisfies the equations

$$A_s |\psi_0\rangle = |\psi_0\rangle, \quad B_p |\psi_0\rangle = |\psi_0\rangle, \quad \forall s, p.$$

Despite its simplicity, the model and its ground state are far from trivial. Let us assume periodic boundary conditions for the system (i.e., it is defined on a torus, hence the first part of its name). The number of star (plaquette) operators equals the number of lattice sites  $N$ . However, not all of them are independent. The product of all star (plaquette) operators is always 1 because it is the trivial product of squares of spin-1/2 (Pauli matrix) operators. (Notice, for instance, that every time we take the product of two neighbouring star operators, the  $\sigma_i^x$  operator shared between them is squared; similarly for plaquette operators.) Therefore, the number of independent star and plaquette operators is  $2N - 2$  whereas the number of degrees of freedom in the system is  $2N$ . Specifying the values of all  $A_s$  and  $B_p$  determines uniquely the energy of the system ( $H$ ) but it *does not* identify a unique state. Rather, it identifies a 4-fold degenerate manifold of states.

In order to resolve the ground state degeneracy one needs to find two additional spin-1/2 like operators that commute with all  $A_s$  and  $B_p$  and yet are not directly dependent on them. One can verify that there are no such operators with local support and we need to consider instead products of an ensemble of spin operators that spans the entire width of the system. For instance, we can use the two loops  $\mathcal{L}_1$  and  $\mathcal{L}_2$  illustrated in Fig. 13 and take the products:

$$\Gamma_1 = \prod_{i \in \mathcal{L}_1} \sigma_i^z \quad \Gamma_2 = \prod_{i \in \mathcal{L}_2} \sigma_i^z. \quad (9)$$

It is straightforward to see that the new operators  $\Gamma_1$  and  $\Gamma_2$  commute with one another and with all  $B_p$  (trivially) and all  $A_s$  operators (the latter is a consequence of the fact that  $\Gamma_{1,2}$  share either two or no spins with any of the star operators). Their eigenvalues  $\pm 1$  completely resolve the degeneracy.

The choice of paths  $\mathcal{L}_1$  and  $\mathcal{L}_2$  is immaterial so long as their respective winding numbers are preserved ( $\mathcal{L}_1$  winds around the torus in one direction once;  $\mathcal{L}_2$  winds once along the other direction). Given two different choices for  $\mathcal{L}_1$ , the product of the two corresponding  $\Gamma_1$  operators is equivalent to the product of all the plaquette operators in between them. In the ground state, the latter are all equal to 1 and so is their product; hence, the two  $\Gamma_1$  operators must have the same eigenvalue. Similarly for  $\mathcal{L}_2$ . (These additional operators are equivalent to winding Wilson loops that the reader may be familiar with from lattice gauge theory.)

Notice that the nature of the degeneracy is not related to the breaking of a symmetry. Indeed, one can show that all local operators have trivial (namely, zero-ranged) correlations. The degeneracy depends on the topology of the system: It is 4-fold on a torus (genus  $g = 1$ ) and it would be in general  $2^{2g}$ -fold on a surface of genus  $g$ . The information that distinguishes one ground state from another is contained in the eigenvalues of the operators  $\Gamma_1$  and  $\Gamma_2$ . These values cannot be determined from knowing the state of any finite subset of spins in the system; we need to know their state for a subset that spans the entire system. Moreover, we have seen that the eigenvalues of  $\Gamma_1$  and  $\Gamma_2$  are independent of the microscopic choice of paths  $\mathcal{L}_1$  and  $\mathcal{L}_2$ ; they depend only on their global properties, namely how they wind around the torus. As such, we say that the system is topologically ordered and the different degenerate states are dubbed topological sectors.

The ability to store quantum information non-locally as a superposition of ground states of this system, inherently protected from local perturbations, is responsible for the great interest in recent years from the quantum information and quantum computing communities (hence the second part of its name).

**Exercise:** check that the choice of  $\sigma^z$  operators in Eq. (9) is arbitrary and one could equally use  $\sigma^x$  operators upon replacing the paths  $\mathcal{L}_1$  and  $\mathcal{L}_2$  on the direct lattice with equivalent paths on the dual lattice. Discuss the action of the new winding operators with respect to the old ones (equivalently, their commutation relations).

Although the toric code is indeed very different from spin ice, an interesting parallel can be drawn between the two systems. Let us consider the eigenvalues  $\pm 1$  of the  $\sigma^x$  operators and let us represent them as arrows pointing from one sublattice to the

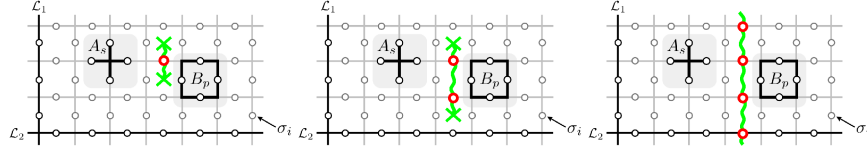


Figure 14: Qualitative illustration of the creation and separation of plaquette type defects in the toric code. A single spin flip creates two negative plaquettes (left panel), which can then separate via the action of other spin flip operations without incurring further energy barriers (middle panel). If the two defective plaquettes wind around the entire system before annihilating, they change the topological sector of the state (right panel).

other (+) and vice versa (-). The star operators in the Hamiltonian favour a ground state where the product of the  $\sigma^x$  operators around each site of the lattice is +1. In the language of the arrows, this corresponds to enforcing an even number of arrows pointing into (equivalently, out of) each site. This is the same as the 2in-2out ice rules in spin ice, with the addition of 4in and 4out tetrahedra. The plaquette operators in the Hamiltonian are kinetic terms with respect to the arrow representation, introducing quantum dynamics into an otherwise classical vertex model. In summary, the toric code ‘looks like’ a quantum spin ice model in 2D with the addition of low-energy 4in and 4out vertices. This addition is however responsible for a major difference in their properties, whereby one system is in a Coulomb phase with an emergent gauge symmetry and the other is in a  $\mathbb{Z}_2$  topologically ordered state.

### 3.2 Elementary excitations

In order to understand the nature of the elementary excitations over the ground state of the toric code, let us consider the action of a  $\sigma_i^x$  operator applied to a given spin  $i$ . While it trivially commutes with the star operators, the value of the  $\sigma^z$  component of the spin is changed and therefore the two plaquette operators that share this spin acquire a negative eigenvalue (Fig. 14, left panel). The energy of the system is correspondingly raised by  $4\lambda_B$ .

In a conventional spin-1/2 ground state, a single spin reversal is typically the lowest energy excitation. Acting with further flipping operators costs increasingly more energy. However, much like spin ice, this is not the case for the toric code. Consider the action of another  $\sigma_j^x$  at a site  $j$  that belongs to one of the two negative plaquettes created by  $\sigma_i^x$ . Having now two spins flipped, the eigenvalue of that plaquette reverts to its lowest energy (positive) state. On the other hand, there is a new plaquette that shares spin  $j$  but not spin  $i$  and its eigenvalue becomes negative. In a nutshell, the action of  $\sigma_j^x$  is to separate the negative plaquettes without introducing any further energetic defects (akin to how appropriate spin flips separate monopoles in nearest neighbour spin ice without any energy cost). This is illustrated in the middle panel of Fig. 14. Therefore, the elementary excitations in the toric code are deconfined plaquettes (equivalently, stars) with negative eigenvalue. Each defect costs an energy  $2\lambda_B$  (equivalently,  $2\lambda_A$ ).

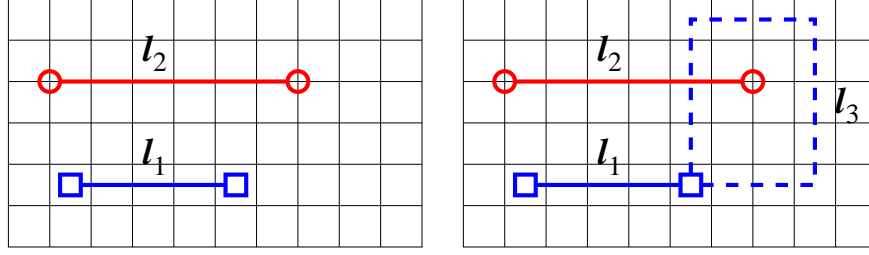


Figure 15: Qualitative illustration of the braiding of a plaquette defect around a star defect.

They can only be created or annihilated in pairs.

In contrast to classical spin ice, we have here two types of excitations: defective stars and defective plaquettes. Whereas they do not interact, they have non-trivial reciprocal statistics. Indeed, let us consider two negative plaquettes  $p$  and  $p'$  on the lattice (they can only be created in pairs and therefore it is not useful to consider only one of them in isolation). In order to create these two excitations from the ground state of the system, one has to choose a path from  $p$  to  $p'$  on the dual lattice and act with the product of all  $\sigma_i^x$  operators along the path (see Fig. 14). One can check that the choice of path is immaterial as any two different paths differ from one another by products of star operators (assuming that there are no star defects in between them). Similar considerations apply to negative star operators at  $s$  and  $s'$ , with respect to paths on the direct lattice from  $s$  to  $s'$  and products of  $\sigma_i^z$  operators. We can now imagine to have two plaquette and two star defects in the system; we keep three of them fixed and we drag, say, one of the plaquettes around one of the star defects (but *not* around the other) and back to its initial position (Fig. 15). The initial and final state are the same in terms of positions of the defects. However, the braiding operation of moving one plaquette around a star necessarily changes the parity of the number of times that the dual path  $p$ - $p'$  intersects the direct path  $s$ - $s'$ . This results in the state of the system acquiring an overall phase factor  $e^{i\pi} = -1$ . Plaquette and star defects have relative *semionic* statistics!

**Exercise:** construct the wave functions of the two states represented in Fig. 15, namely  $|\psi_{\text{left}}\rangle = \prod_{i \in l_1} \sigma_i^x \prod_{j \in l_2} \sigma_j^z |\psi_0\rangle$  and  $|\psi_{\text{right}}\rangle = \prod_{i \in (l_1 \cup l_3)} \sigma_i^x \prod_{j \in l_2} \sigma_j^z |\psi_0\rangle$ . Using the well known (anti)commutation relations between Pauli matrices, show that the two states are indeed identical up to an overall minus sign.

The emergence of quasiparticles with fractional statistics with respect to the microscopic degrees of freedom in the system is another instance of fractionalisation in topologically ordered systems.

### 3.3 Dynamics

Once defective stars and plaquettes are created in the system, they are static in so far as the action of the Hamiltonian is concerned. None of the operators in Eq. (8) can

alter their position or their value. Defects acquire dynamics only if we assume that either thermal or quantum fluctuations are present, which generally couple to  $\sigma^x$  and  $\sigma^z$  operators (as well as  $\sigma^y$ , but we shall not discuss that case in these notes). In presence of such fluctuations, the defects are able to move freely across the system. Once again, similarly to spin ice, defects act as dynamical facilitators for the system's response and relaxation. Spin flips that result in the hopping of a defect do not incur an energy barrier; whereas generic spin flips away from existing defects must overcome the energy barrier to create two new excitations.

Contrary to spin ice, where the role of the defects as dynamical facilitators is readily reflected in the magnetic response of the system (e.g., its susceptibility), the case of the toric code is more subtle due to the lack of any local correlations. Here we discuss how the dynamics of the excitations relates to the topological properties of the system.

Let us prepare the system in a given topological sector. The creation, say, of a pair of defective plaquettes only disrupts the spins along the path that was chosen to generate them. Away from this path, the eigenvalues of the winding loop operators in Eq. (9) remain unaltered. Once fluctuations allow the defective plaquettes to move around, the eigenvalues of the winding loop operators are statistically well defined only if the two plaquettes remain close to one another. Once they separate and wander across the system, the information about the initial topological sector is lost. Indeed, if we create a pair of negative plaquettes, wind them around the system, and then we annihilate them, the outcome is that all winding loop operators crossing the winding path of the plaquettes change sign and the topological sector of the system changes (Fig. 14, right panel).

In order to understand how a defect-driven change in topological sector takes place dynamically, let us take a look at the shape of the relevant energy barrier. Starting from the ground state, the system faces an energy increase for the creation of two defects ( $\Delta = 4\lambda_A$  or  $\Delta = 4\lambda_B$ , depending on the type of defect). The energy remains then constant as the defects move about. In order to change topological sector, one of the defects has to separate from the other and wind around the system before they annihilate. As a result, the width of the barrier is of the order of the system size  $L$ , after which the energy decreases again to the GS value upon annihilating the two defects. The shape of such barrier is depicted in Fig. 16.

Local quantum fluctuations can induce a change in topological sector by exciting a virtual pair of defects and make them hop (whilst the system is in a virtual excited state) across the entire lattice before they annihilate and the energy is finally lowered. If the strength of the quantum fluctuations that couple to the  $\sigma_i^x$  operators is  $t$ , then the height  $\Delta$  and width  $\sim L$  of the barrier imply that the quantum tunnelling under the barrier is a perturbative process of order  $L$  in  $t/\Delta$ . The tunnelling rate  $\sim (t/\Delta)^L$  is therefore exponentially suppressed in the size of the system. Correspondingly, the relaxation time scale from one topological sector to another due to local quantum fluctuations grows exponentially with system size,  $\tau_Q \sim \exp[L \ln(\Delta/t)]$ .

This is to be contrasted with the analogous process in presence of thermal fluctuations. Once a pair of (real) defects has been thermally excited against the energy cost  $\Delta$ , they are now free to diffuse across the system. The probability that they wind around the system and then they annihilate is related to the first passage probability of a random walk to come back to the origin after winding around the torus an odd number

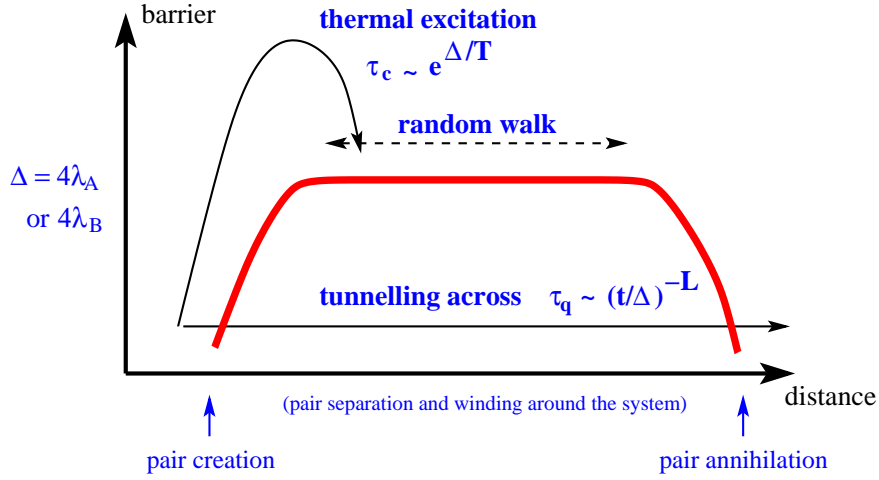


Figure 16: Qualitative illustration of the shape of the energy barrier to change topological sector in the toric code via defect creation, diffusion, and annihilation. The arrows represent thermal and quantum processes, with their relevant time scales.

of times, which is polynomial in  $L$ . The overall probability of the process is therefore given by the product of the activation probability  $\exp(-\Delta/T)$  times a factor that does not depend on  $\Delta$  or  $T$  and that scales polynomially in system size,  $\tau_C \sim e^{\Delta/t} \text{Poly}(L)$ .

Whether thermal or quantum processes are the dominant contribution in the thermal relaxation of the system is thus a matter of order of limits. In a system of finite size, there is a temperature below which the exponential slowing down of thermal processes due to the activation barrier exceeds the exponential suppression in system size of quantum tunnelling and the latter becomes the faster process ( $\tau_Q \ll \tau_C$ ). On the other hand, if the system becomes larger and larger at fixed temperature, the protection from quantum fluctuations is bound to become far greater than the protection from thermal fluctuations, and the latter become the faster relaxation channel ( $\tau_Q \gg \tau_C$ ). A more general discussion of quantum vs thermal relaxation processes and their relation to (topological) quantum glassiness can be found in Ref. [39].

It is worth commenting that relaxation times which scale polynomially in system size are unusual in ordered phases and signal a remarkable weakness. Whereas quantum topological order in the toric code is highly robust to quantum perturbations, it is immediately lost (in the thermodynamic limit) when the system is coupled to a thermal bath. This issue is discussed in detail in Refs. [34, 35, 36]. Furthermore, Ref. [37] uses numerical simulations to investigate the relaxation dynamics of the toric code coupled to a thermal bath and discusses its connection to thermal fragility.

### 3.4 Intriguing comparison: Kinetically Constrained Models

As illustrated in the examples above, the appearance of topologically ordered phases (in lattice models) is closely related to the presence of dominant energy terms that enforce



local constraints (cf. dimer / vertex / plaquette constraints). Albeit insufficient to drive the system into a conventionally ordered phase, these terms are directly responsible for the non-trivial global properties of the system.

It is interesting to draw a parallel between the role of local constraints in topologically ordered systems and another area of research, namely that of *Kinetically Constrained Models* (KCM) [1], where local constraints are used instead to induce non-trivial dynamical properties (i.e., unusually slow response and equilibration whereas the thermodynamic properties remain altogether trivial).

Kinetically constrained models received much attention in the literature as an attempt to understand the emergence of long relaxation time scales and glassiness in systems without disorder.

Here we briefly review two examples and we comment on their analogies and differences with respect to the topologically ordered systems considered earlier. We limit our discussion to classical 2D systems, although higher dimensional [48] as well as quantum [38, 39] examples are also available.

### 3.4.1 Square lattice plaquette model

The first model we consider is an Ising model on the square lattice (with spins living on the sites, not the bonds) and Hamiltonian [40]:

$$H = -J \sum_p \prod_{i \in p} S_i \quad (J > 0), \quad (10)$$

where  $p$  labels the plaquettes on the lattice and  $\prod_{i \in p} S_i$  is the product of the 4 spins at the corners of plaquette  $p$ . It belongs to a broader class of models known as *gonihedric* models and it is also directly mappable onto Baxter's eight-vertex model (notice the direct correspondence with the toric code).

The system does not exhibit any phase transitions as a function of temperature and the high temperature paramagnetic phase is continuously connected to the low temperature phase where all plaquettes have the same sign ( $\prod_{i \in p} S_i = +1$  for  $J > 0$ ). This is most straightforwardly seen in the language of the dual variables  $\tau_p \equiv \prod_{i \in p} S_i$ , defined on the centres of the plaquettes of the original lattice, where the Hamiltonian reduces to that of a trivial paramagnet,

$$H = -J \sum_p \tau_p. \quad (11)$$

Notice that the Hamiltonian in Eq. (10) is invariant under transformations that flip straight lines of spins on the direct lattice, spanning the entire system (notice the analogies and differences with the winding loops introduced in the discussion of the toric code). This invariance has two important consequences. Firstly, the zero temperature limit when all plaquettes are polarised is sub-extensively degenerate (namely, the number of degenerate configurations scales with the exponential of the linear size  $L$  of the system rather than the exponential of the volume  $L^2$ ). Secondly, all two-spin correlators

$$\langle S_i S_j \rangle = \sum_{\{S_k\}} S_i S_j \frac{e^{-\beta H}}{Z} \quad Z = \sum_{\{S_k\}} e^{-\beta H} \quad (12)$$

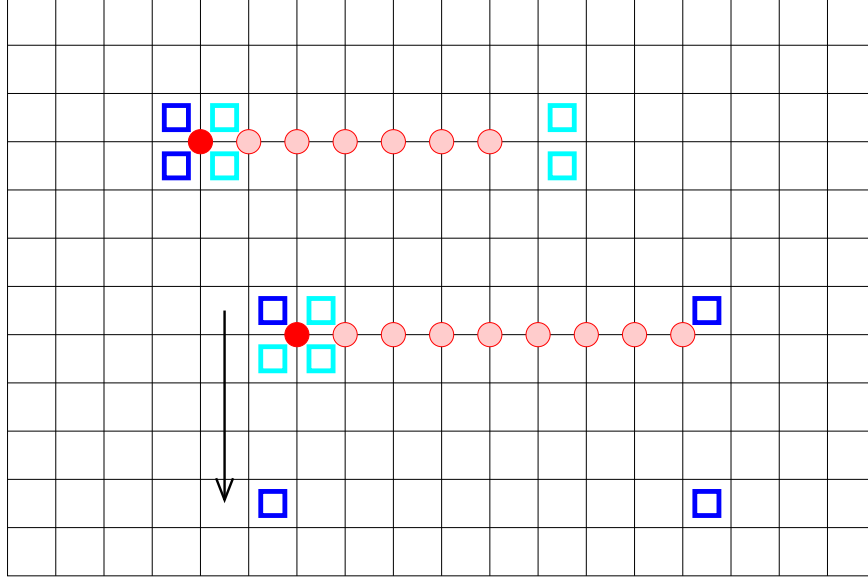


Figure 17: Illustration of defects in the square plaquette model. A single spin flip changes the sign of the 4 plaquettes it belongs to, which are then pairwise free to move along straight lines across the system. The bottom portion of the figure illustrated how isolated defects are brought together to eventually annihilate, as the system attempts to reach one of its defect-less ground states via the allowed (constrained) defect dynamics.

vanish identically at all temperatures. This is because there is always at least one straight line (either horizontal or vertical or both) that goes through spin  $i$  but not spin  $j$ . Therefore, the correlators vanish by symmetry (so long as the system remains ergodic).

If the duality transformation trivialises the thermodynamics of the system, the dynamical processes become then nontrivial. At low temperature, in order to transition from one lowest energy configuration to another, the system must overcome an energy barrier that is similar to the one encountered in the toric code. Firstly, a thermally excited spin creates four defective plaquettes ( $\Delta = 8J$ ). Then neighbouring spins can flip to annihilate two defective plaquettes and create two new ones, thus effectively separating the four defective plaquettes in pairs without changing the energy of the system (see Fig. 17). Contrary to the toric code however, the motion must follow a straight line. If the pairs wind around the system before they annihilate, the system ends in a new lowest energy configuration. Once again, we expect relaxation time scales that are exponential in the height of the barrier over the temperature,  $\exp(\Delta/T)$ , times a temperature independent factor that scales polynomially with the system size.

Although we considered the time scale for the system to relax from one lowest energy state to another, similar arguments apply to the relaxation time scales in the system as the temperature is progressively reduced (see e.g., Ref. [40]).

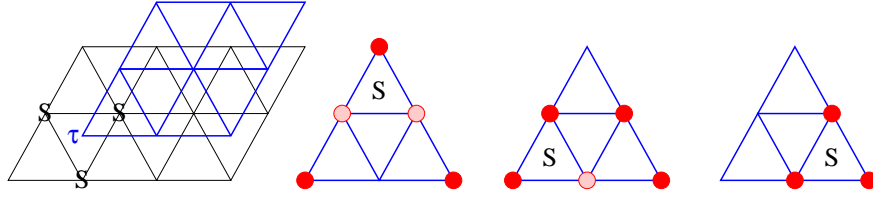


Figure 18: Illustration of the original triangular lattice of the  $S$  spins and the dual triangular lattice of the  $\tau$  spins (left panel, black and blue lattices, respectively). The rightmost three panels represent the steps (from left to right) to annihilate 3 defective plaquettes at the corners of a dual triangle of side 2, by flipping three  $S$  spins in sequence. Notice that in the process we cannot avoid to create one additional defect.

### 3.4.2 Triangular lattice plaquette model

The second model we consider is similar to the former defined on the triangular lattice (again, with Ising spins living on the sites). The Hamiltonian of the system can be written as [41]

$$H = J \sum_{\nabla} \prod_{i \in \nabla} S_i \quad (J > 0), \quad (13)$$

where  $\nabla$  labels the downward-pointing triangular plaquettes and  $\prod_{i \in \nabla} S_i$  is the product of the three Ising spins at their three vertices. (This is similar but not to be confused with the Baxter-Wu model, which includes upward as well as downward pointing triangles.)

The thermodynamic properties of the system are best understood in terms of dual variables  $\tau_{\nabla} \equiv \prod_{i \in \nabla} S_i$ , which live on the triangular lattice formed by the centres of the downward pointing triangles in the original lattice (Fig. 18, left panel). If the linear dimension of the system is a power of 2 (i.e.,  $L = 2^n$ ,  $\exists n \in \mathbb{N}$ ) and periodic boundary conditions are assumed, one can show that there is a one-to-one correspondence between the two representations of the system [41]. In the new language, the Hamiltonian becomes

$$H = J \sum_{\nabla} \tau_{\nabla}, \quad (14)$$

i.e., that of an ensemble of noninteracting spins in an applied magnetic field. In the dual language, it is straightforward to write the partition function of the system and use the mapping to obtain correlation functions of the original degrees of freedom [3]. The system does not undergo a phase transition as a function of temperature and the lowest energy configuration (where all  $\tau_{\nabla} = -1$ ) is continuously connected to the trivial paramagnetic phase.

Whereas the duality transformation allows to demonstrate straightforwardly the trivial thermodynamics of the system, the dynamical processes become nontrivial. Flipping an individual spin of the original system ( $S$ ) now leads to changing the sign (i.e., flipping) the three plaquette variables ( $\tau$ ) that share the spin (Fig. 18). One should

contrast this to the corresponding defect dynamics in the toric code (where, e.g., flipping a bond spin changes the sign of the two adjacent star or plaquette operators) and of the square lattice plaquette model (where flipping a site spin changes the sign of four plaquettes). Notice that the  $S$  spins live only in the *upward pointing* triangular plaquettes of the  $\tau$  spin lattice.

The presence of such dynamical constraints plays a crucial role in the response and equilibration properties of the system, which become drastically different from the ones expected for a trivial paramagnet in an applied field. Similarly to the square plaquette model, Monte Carlo simulations show the emergence of unusually long relaxation time scales and glassiness at low temperatures [41]. However, the behaviour in this case is remarkably different from the activated behaviour encountered in the toric code and in the square plaquette model, as the characteristic time scale grows exponentially with the *square of the inverse temperature* [41, 3, 5].

In order to understand this behaviour, let us consider how the system approaches the lowest energy state upon lowering the temperature. For this purpose, it is sufficient to consider the lowest energy excitations above the ground state where all  $\tau_{\nabla} = -1$ . It is possible to show that these excitations take the form of equilateral triangles of linear size  $\ell = 2^k$ , with  $k$  integer, that have single isolated defects  $\tau_{\nabla} = +1$  at each of their three vertices, as illustrated in Fig. 18. (The proof is given in detail in Ref. [41] and will not be reported here.)

These defect structures are metastable, in that they cannot be removed (or moved) without incurring an energy cost. The steps towards the annihilation of a structure with  $k = 1$  are explicitly shown in Fig. 18. They require flipping three original ( $S$ ) spins, which in turn flip three plaquette ( $\tau$ ) spins each. In the process, we generate one more defect than the three we started with and the overall energy barrier is therefore  $2J$ .

The same process can be iterated for larger defect structures: to annihilate a structure of linear size  $2^k$  one has to annihilate the three structures of linear size  $2^{k-1}$  within it, which requires overcoming the barrier to create one extra defect,  $2J$ . Similarly for each of the structures of linear size  $2^{k-1}$ , etc. Until we arrive at  $k = 1$ , where the process above applies. The overall barrier is thus  $\Delta = 2Jk = 2J \log_2(\ell)$ , where  $\ell$  is the initial separation between defects.

***Exercise:*** follow the discussion in the text to prove that the smallest number of additional intermediate defects that one ought to create in order to annihilate three defective plaquettes at the corners of an equilateral triangle of side  $2^k$  is  $k$ .

In thermodynamic equilibrium, the average separation between defects scales as the inverse square root of their density, namely  $\ell \sim \exp(J/T)$  since from Eq. (14) we see that the energy cost of a defect is  $2J$  whence their density is  $\sim \exp(-2J/T)$ . Therefore,  $\Delta = 2J \log_2(\exp(J/T))$  and the corresponding relaxation time scale is  $\tau \sim \exp(\Delta/T) \sim \exp(2J^2/T^2 \ln 2)$ .

Even though it is still the case that relaxation time scales diverge only in the zero temperature limit, the plaquette energy terms on the triangular lattice achieve a qualitatively different behaviour than the square lattice. They give rise to an unusually strong slowing down which is exponential in the square of the inverse temperature. This is a substantial improvement in robustness to thermal fluctuations. One might thus wonder whether new lattice models can be designed where an appropriate combination of pla-

quette energy terms manages to achieve, say, topological order as in the toric code and exponential inverse temperature square protection from thermal fluctuations, as in the triangular plaquette model. In this case, the enhance protection would not be thermodynamic (in the sense of topological order surviving up to a finite temperature phase transition) but rather dynamical, slowing down the destabilising thermal defects into a nearly glassy state.

### 3.4.3 Quantum kinetically constrained models

Quantum versions of kinetically constrained models also exist, although their discussion is beyond the scope of these short lectures. They are in general less studied and less well understood than their classical counterparts. Some examples are discussed in Ref. [39], covering both two-dimensional and three-dimensional cases that exhibit energy barriers and quantum relaxation rates akin to the ones illustrated in Fig. 16.

Similarly to the case of the toric code model, one finds that large but low energy barriers are effective at slowing down quantum tunnelling processes (exponentially suppressed in the width of the barrier), yet they are rather ineffective with respect to thermal fluctuations (exponentially suppressed in the height of the barrier but only polynomially suppressed in the width). This leads to an interesting parallel between classical and quantum glassiness, and the fact that (topological) quantum glassiness can be a behaviour inherent to zero-temperature, which disappears immediately at any finite temperature [39].

As suggested in these notes, it is often found that a rich dynamical phenomenology in quantum kinetically constrained models is accompanied by the emergence of quantum topological order. In their dual description, quantum kinetically constrained models can be seen once again as models of point-like particles that move on a lattice according to allowed and disallowed processes. Other models that typically exhibit topological properties are those where particle hopping processes are accompanied by non-trivial phase factors (see e.g., Haldane’s model, fractional Chern insulators, and the recent artificial gauge fields in ultracold atomic systems). It will be interesting to investigate how quantum kinetically constrained models behave when similar phase factors are present in the allowed dynamical processes.

## 4 Conclusions

In summary, we have discussed a few examples of how systems with topological properties behave out of equilibrium. The topological nature of the low energy state in these systems is closely related to the fractionalised character of its elementary excitations. In turn, we have seen that these excitations are directly responsible for the response and equilibration behaviour. This intriguing interplay gives rise to a rich variety of exciting phenomena that we are just beginning to understand and classify.

In the context of statistical mechanical models such as classical spin ice, we have shown how the nature of the low temperature phase and its excitations reflects in reaction-diffusion relaxation processes with local and global kinematic constraints as well as emergent long range Coulomb interactions. Spin ice thus offers a realisation

of several paradigmatic concepts in nonequilibrium dynamics, with an unusually high degree of tunability.

We also discussed how a similar interplay between the topological ground state and its fractionalised excitations leads to interesting equilibration properties in quantum mechanical systems, in presence of both quantum and thermal perturbations. However, the additional complexity of out of equilibrium quantum mechanics in strongly interacting systems limits the discussion at present to somewhat simple examples (e.g., the toric code) and achieves a far less detailed understanding than its classical counterpart (e.g., spin ice, kinetically constrained models). Notwithstanding, one encounters interesting scenarios demonstrating the interplay of topological order and glassiness, which raise intriguing questions. Quantum topological order appears to be more susceptible to thermal fluctuations than conventional (local) types of order, at least in two and three dimensions. Could topological protection be improved by slowing down (thermal) defects, i.e., freezing them out in a glassy state? Can this be achieved without disorder, using fractal structures as, e.g., in the kinetically constrained triangular plaquette model?

Overall, this is an exciting and timely research direction, also thanks to recent material and technological developments that are producing an increasing number of experimental results on systems with topological properties out of equilibrium.

## Acknowledgements

This work was supported in part by EPSRC Grant EP/K028960/1.

## References

- [1] F. Ritort and P. Sollich, *Adv. Phys.* **52**, 219 (2003).
- [2] J. P. Garrahan and D. Chandler, *Proc. Natl. Acad. Sci.* **100**, 9710 (2003).
- [3] J. P. Garrahan and M. E. J. Newman, *Phys. Rev. E* **62**, 7670 (2000).
- [4] A. Buhot and J. P. Garrahan, *Phys. Rev. Lett.* **88**, 225702 (2002).
- [5] J. P. Garrahan, *J. Phys. Cond. Matt.* **14**, 1571 (2002).
- [6] X.-G. Wen, *Int. J. Mod. Phys. B* **4**, 239 (1990).
- [7] X.-G. Wen, *Adv. Phys.* **44**, 405 (1995).
- [8] A. Y. Kitaev, *Ann. of Phys.* **303**, 2 (2003).
- [9] J. von Neumann, *Göttinger Nachrichten*, 245 (1927).
- [10] X.-G. Wen, *Phys. Rev. B* **65**, 165113 (2002).
- [11] C. Castelnovo, C. Chamon, and D. Sherrington, *Phys. Rev. B* **81**, 184303 (2010).

- [12] C. Castelnovo, R. Moessner, and S. L. Sondhi, *Nature* **451**, 42 (2008).
- [13] S. T. Bramwell, S. R. Giblin, S. Calder, R. Aldus, D. Prabhakaran, and T. Fennell, *Nature* **461**, 956 (2009).
- [14] D. Toussaint and F. Wilczek, *J. Chem. Phys.* **78**, 2642 (1983)
- [15] V. V. Ginzburg, L. Radzihovsky, and N. A. Clark, *Phys. Rev. E* **55**, 395 (1997).
- [16] J. Snyder, B. G. Ueland, J. S. Slusky, H. Karunadasa, R. J. Cava, and P. Schiffer, *Phys. Rev. B* **69**, 064414 (2004).
- [17] I. A. Ryzhkin, *JETP* **101**, 481 (2005).
- [18] C. Castelnovo, R. Moessner, and S. L. Sondhi, *Phys. Rev. B* **84**, 144435 (2011).
- [19] G. Sala, M. J. Gutmann, D. Prabhakaran, D. Pomaranski, C. Mitchelitis, J. B. Kycia, D. G. Porter, C. Castelnovo and J. P. Goff, *Nature Mat.* **13**, 488 (2014).
- [20] C. Castelnovo, R. Moessner, and S. L. Sondhi, *Annu. Rev. Condens. Matter Phys.* **3**, 35 (2012).
- [21] S. T. Bramwell and M. J. P. Gingras, *Science* **294**, 1495 (2001).
- [22] M. J.P. Gingras and P. A. McClarty, *Rep. Prog. Phys.* **77**, 056501 (2014).
- [23] L. D. C. Jaubert and P. C. W. Holdsworth, *Nature Phys.* **5**, 258 (2009).
- [24] S. R. Giblin, S. T. Bramwell, P. Holdsworth, D. Prabhakaran, and I. Terry, *Nature Phys.* **7**, 252 (2011).
- [25] J. A. Quilliam, I. R. Yaraskavitch, H. A. Dabkowska, B. D. Gaulin, and J. B. Kycia, *Phys. Rev. B* **83**, 094424 (2011).
- [26] K. Matsuhira, et al., *J. Phys. Soc. Jpn* **80**, 123711 (2011).
- [27] L. R. Yaraskavitch, et al., *Phys. Rev. B* **85**, 020410 (2012).
- [28] H. M. Revell, et al., *Nature Phys.* **9**, 34 (2013).
- [29] V. Kaiser, S. T. Bramwell, P. C. W. Holdsworth, R. Moessner, *Nature Mat.* **12**, 1033 (2013).
- [30] L. Onsager, *J. Chem. Phys.* **2**, 599 (1934).
- [31] C. Castelnovo, R. Moessner, S. L. Sondhi, *Phys. Rev. Lett.* **104**, 107201 (2010).
- [32] A. J. Bray, *Adv. in Physics* **43**, 357 (1994).
- [33] S. Mostame, C. Castelnovo, R. Moessner, and S. L. Sondhi, *PNAS* **111**, 640 (2014).
- [34] C. Castelnovo and C. Chamon, *Phys. Rev. B* **76**, 184442 (2007).



- [35] C. Castelnovo and C. Chamon, *Phys. Rev. B* **78**, 155120 (2008).
- [36] Z. Nussinov and G. Ortiz, *PNAS* **106**, 16944 (2009); *Annals of Physics* **324**, 977 (2009).
- [37] C. D. Freeman, C. M. Herdman, D. J Gorman, K. B. Whaley, arXiv:1405.2315 (2014).
- [38] C. Chamon, *Phys. Rev. Lett.* **94**, 040402 (2005).
- [39] C. Castelnovo and C. Chamon, *Phil. Mag.* **92**, 304 (2011).
- [40] A. Lipowski, *J. Phys. A: Math. Gen.* **30**, 7365 (1997).
- [41] M. E. J. Newman and C. Moore, *Phys. Rev. E* **60**, 5068 (1999).
- [42] Y. Levin, *Rep. Prog. Phys.* **65**, 1577 (2002).
- [43] D. J. P. Morris, D. A. Tennant, S. A. Grigera, B. Klemke, C. Castelnovo, R. Moessner, C. Czternasty, M. Meissner, K. C. Rule, J.-U. Hoffmann, K. Kiefer, S. Gerischer, D. Slobinsky, and R. S. Perry, *Science* **326**, 411 (2009).
- [44] H. Takatsu, K. Goto, H. Otsuka, R. Higashinaka, K. Matsubayashi, Y. Uwatoko, and H. Kadowaki, *J. Phys. Soc. Japan* **82**, 104710 (2013).
- [45] D. Slobinsky, C. Castelnovo, R. A. Borzi, A. S. Gibbs, A. P. Mackenzie, R. Moessner, and S. A. Grigera, *Phys. Rev. Lett.* **105**, 267205 (2010).
- [46] C. Paulsen, et al., *Nature Phys.* **10**, 135 (2014).
- [47] M. J. Jackson, et al., *Phys. Rev. B* **90**, 064427 (2014).
- [48] D. A. Johnston, A. Lipowski, Ranasinghe, and P. K. C. Malmi, Chapter 7 in *Rugged Free-Energy Landscapes - An Introduction*, Springer Lecture Notes in Physics, 736, ed. W. Janke, (2008).